Vertical Mixing and the Temperature and Wind Structure of the Tropical Tropopause Layer

Thomas J. Flannaghan * and Stephan Fueglistaler

Atmosphere Ocean Sciences, Princeton University, Princeton, New Jersey

* *Corresponding author address:* Thomas Flannaghan, 300 Forrestal Road, Sayre Hall, Princeton University, Princeton, NJ 08540.

E-mail: tomflannaghan@gmail.com

ABSTRACT

We show that vertical mixing can lead to significant momentum and heat fluxes in the tropical tropopause layer (TTL) and that these momentum and heat fluxes can force large climatological temperature and zonal wind changes in the TTL. We present the climatology of vertical mixing and associated momentum and heat fluxes as parametrised in the European Centre for Medium Range Weather Forecasting (ECMWF) Interim reanalysis and as parametrised by the mixing scheme currently used in the ECMWF operational analyses. Each scheme produces a very different climatology showing that the momentum and heat fluxes arising from vertical mixing are highly dependent on the scheme used. A dry GCM is then forced with momentum and heat fluxes similar to those seen in ERA-Interim to assess the potential impact of such momentum and heat fluxes. We find a significant response in the TTL, leading to a temperature perturbation of approximately 4 K, and a zonal wind perturbation of approximately 12 $\mathrm{m\,s^{-1}}$. These temperature and zonal wind perturbations are approximately zonally symmetric, are approximately linear perturbations to the unforced climatology, and are confined to the TTL between approximately 10°N and 10°S. There is also a smaller amplitude tropospheric component to the response. Our results indicate that vertical mixing can have a large but uncertain effect on the TTL, and that choice and impact of the vertical mixing scheme should be an important consideration when modelling the TTL.

1. Introduction

Vertical mixing in the free atmosphere has been observed to occur in the tropical tropopause layer (TTL) (Fujiwara et al. 1998; Fujiwara and Takahashi 2001; Fujiwara et al. 2003), with observations indicating substantial exchanges between troposphere and stratosphere due to mixing. The TTL plays an important role in the global climate system (Fueglistaler et al. 2009a), and as such it is fair to ask to what extent vertical mixing could affect the TTL structure.

Fueglistaler et al. (2009b) and Flannaghan and Fueglistaler (2011) find that vertical mixing in the European Centre for Medium Range Weather Forecasting (ECMWF) Interim reanalysis (ERA-Interim) (Simmons et al. 2007; Dee et al. 2011) leads to significant diabatic terms in the TTL. Wright and Fueglistaler (2013) showed that vertical mixing is also important for the diabatic heat budget in other reanalysis datasets, and noted that there are large discrepancies between reanalyses. These studies focused on the heat budget, and therefore temperature tendency, but as noted in Flannaghan and Fueglistaler (2011) there is also a significant momentum forcing due to mixing in ERA-Interim, and so in this study we shall consider the effect of both temperature tendency and momentum forcing.

We shall use two different mixing parametrisation schemes in this study; the scheme used in ERA-Interim and a second scheme that is used in more recent ECMWF models. These two schemes are fundamentally quite different (as discussed in Flannaghan and Fueglistaler (2011)), and give very different results, showing that the forcing terms associated with mixing are highly uncertain. Given the uncertain nature of the forcing that vertical mixing exerts on the atmosphere, it is important to understand the potential impact such terms may have on the atmosphere.

We shall begin by presenting the climatology of the forcing terms generated by each mixing scheme in section 2 and then go on to present the impact of these forcing terms on the TTL climatological temperature and wind in an idealized model in section 3, followed by an analysis of the model results in section 4.

2. Climatology of mixing

We use ERA-Interim 6 hourly data on a 1° grid on pressure levels chosen to be close to ERA-Interim model levels. For the layer of interest here (the TTL), these pressure levels are very close to, and from the 80 hPa level upwards identical with, the original model levels, such that interpolation errors are minimal.

We shall apply two different mixing schemes that are used by ECMWF in the Integrated Forecast System (IFS); the revised Louis (rL) scheme (Louis 1979; Viterbo et al. 1999) and the Monin-Obukhov (MO) scheme as used in current operational analyses (both are defined in Part IV of the IFS documentation.) The definitions of the schemes used in this study are given in full in the Appendix and are also discussed in Flannaghan and Fueglistaler (2011). Both schemes parametrise mixing as a diffusive term, with the diffusivity K referred to here and in the literature as the exchange coefficient. Both schemes allow K to vary as a function of Richardson number Ri defined in terms of the model temperature and wind fields as

$$Ri = \frac{N^2}{|\partial \mathbf{u}/\partial z|^2}, \tag{1}$$

where N^2 is the static stability and $\mathbf{u}$ is the horizontal wind (u, v).

The MO scheme (or similar variants) is commonly used in global climate models and forecast models, and has the key property that mixing only occurs when the Richardson number Ri falls below approximately 0.25. The rL scheme is used in the IFS models in the lower troposphere, and prior to Cycle 33r1 (introduced in 2008; ERA-Interim is prior to Cycle 33r1) used throughout the free atmosphere, and unlike the MO scheme has a long tail of non-zero K as $Ri \to \infty$. Flannaghan and Fueglistaler (2011) showed that the long tail of the rL scheme leads to very different mixing than that produced by the MO scheme with a cut-off of mixing at $Ri = 0.25$. We shall not discuss which scheme gives a better representation of mixing in the TTL, and such a question is non-trivial; the MO scheme *seems* most physical as it features the observed Richardson number cut-off associated with Kelvin-Helmholtz instability, but when gravity waves are not resolved, and therefore not included when computing the Richardson number, using such a cut-off is problematic. Gravity waves are expected to reduce Richardson number, and therefore increase mixing. This mixing is missed when a cut-off at $Ri = 0.25$ is used where Ri is computed without including gravity waves.

Both mixing schemes are applied offline to ERA-Interim data. Flannaghan and Fueglistaler (2011) find that applying the ERA-Interim mixing scheme offline matches the diabatic residual output given by ERA-Interim in regions with little convection (where the contribution of mixing is well separated from other diabatic terms in the residual) and so we have confidence in computing mixing offline. See the Appendix for more details and validation of the offline calculation method. We were not able to validate the zonal acceleration forcing exerted on the atmosphere by mixing (due to lack of information on the momentum terms), but we assume that the zonal acceleration forcing can also be computed offline, as the calculations performed are very similar to that for the heating due to the mixing scheme.

a. Zonal mean forcing terms

Figure 1 shows the climatological (1989–2009) annual and seasonal (DJF and JJA) average zonal mean zonal acceleration $\overline{X}$ (where $\bar{\cdot}$ denotes the zonal mean) and the temperature tendency $\overline{Q}$ averaged over the inner tropics (10°N–10°S), calculated offline from ERA-Interim temperature and wind using the rL and MO schemes.

Using the rL scheme, both the zonal mean zonal acceleration and the zonal mean temperature tendency have a strong dipole structure in both DJF and JJA, centered at approximately 110 hPa. Zonal mean zonal acceleration is largest in JJA, where the dipole has an amplitude of approximately 0.2 $\mathrm{m\,s^{-1}\,day^{-1}}$ when averaged over the inner tropics. In DJF, dipole structure of the zonal mean zonal acceleration has the opposite sign, and a lower amplitude of approximately 0.1 $\mathrm{m\,s^{-1}\,day^{-1}}$. As a consequence of the change in sign from

DJF to JJA, $\overline{X}$ averaged over the whole period is small everywhere. Zonal mean temperature tendency computed using the rL scheme has a similar structure in both DJF and JJA, with a maximum amplitude of 0.08 $\mathrm{K\,day^{-1}}$ at approximately 90 hPa. $\overline{Q}$ averaged over the whole period has a strong dipole structure. Using the MO scheme, the zonal mean zonal acceleration and zonal mean temperature tendency are both small everywhere, except for the case of zonal mean zonal acceleration in DJF, where we see a dipole structure similar to that when the rL scheme is used.

Figure 2 shows the zonal mean latitudinal structure of the forcing terms due to mixing using the rL scheme. Except for zonal acceleration during DJF, the vertical dipole structures shown in Figure 1 are clearly visible in Figure 2, and are confined to the inner tropics (10°N–10°S) with a very symmetric meridional structure about the equator. Note that the dipole produced by the MO scheme in zonal acceleration in DJF also shows a similar latitudinal structure (not shown).

Wright and Fueglistaler (2013) show similar dipole structures to those presented in Figure 2 in the average (over all months) zonal mean diabatic heating term in the NCEP, CFSR and JRA reanalyses (see their Figure 6), while MERRA's diabatic heating from vertical mixing is much smaller. The diabatic heating due to mixing in NCEP has a larger magnitude of approximately 0.1 $\mathrm{K\,day^{-1}}$ compared to ERA-Interim (approximately 0.05 $\mathrm{K\,day^{-1}}$ over the inner tropics; see black curve in Figure 1b) and has a broader meridional structure. Both CFSR and JRA have dipole structures confined to the inner tropics with typical magnitudes of approximately 0.03 $\mathrm{K\,day^{-1}}$ in the annual mean value (approximately half the value in ERA-Interim), and with a similar form to that in ERA-Interim.

b. Zonal structure in the forcing terms

As shown by Flannaghan and Fueglistaler (2011), both schemes have very zonally asymmetric distributions of exchange coefficients in the TTL. Here, we shall give the full structure of the exchange coefficient K_{H} and the resulting forcing terms X and Q. We begin with the rL scheme before presenting results using the MO scheme. Figure 3 shows DJF and JJA averages of K_{H} computed over 1989 to 2009 using ERA-Interim data. The K_{M} climatology is very similar and not shown here (the Ri dependence of K_{H} and K_{M} is slightly different; see Appendix.) In DJF, mixing occurs primarily at around 104 hPa with three main regions of mixing (shown on the figure) over the Maritime Continent (region A), the central Pacific (region B) and eastern Pacific (region C). In JJA, mixing occurs predominantly over the Indian Ocean and is co-located with the easterlies associated with the Monsoon circulation. The mixing in JJA has a deeper vertical structure, with the peak mixing occurring in the layer centered at 122 hPa.

Figure 4 shows the resulting Q and X averaged over the same region and time period as in Figure 3. In DJF, Q and X are dominated by dipole structures centered at 95 hPa over the Maritime Continent (region A) and the Eastern Pacific (region C). Q has a peak magnitude of approximately 0.3 $\mathrm{K\,day^{-1}}$, and X has a peak magnitude of approximately 1 $\mathrm{m\,s^{-1}\,day^{-1}}$. In the zonal mean, there is a high degree of cancellation in X as the dipole structures over the Maritime Continent (region A) and the Eastern Pacific (region C) have opposite signs, due to the opposite sign in the background wind shear. Conversely, the dipoles in Q have the same sign and therefore reinforce each other, explaining the difference in structure between Figure 2a(i) and (ii). There is no significant temperature tendency or zonal acceleration in the central Pacific (region B) due to low background shear and low background N^2 here. In JJA, X and Q are largest over the Indian Ocean region, with a single large dipole structure centered at 70°E and 113 hPa in both Q and X.

Application of the MO scheme to ERA-Interim data gives a very different climatology. Figure 5 shows the climatology of K_{H} computed using the MO scheme. When using the MO scheme, mixing predominantly occurs in the central Pacific (region B) in DJF, with a maximum exchange coefficient of approximately 10 $\mathrm{m^2\,s^{-1}}$. This K_{H} is much higher than that under the rL scheme (due to difference in nominal mixing lengths between the schemes; see Appendix), and in this case does result in a small localized zonal acceleration term in this region. Mixing in this region is often very sporadic and is often associated with near zero or negative N^2. The substantial $\overline{X}$ term in Figure 1a is due to the mixing over the Central Pacific (region B) and also the weaker mixing over the Eastern Pacific (region C). These two regions of mixing have the same sign, and therefore reinforce in the zonal mean, giving rise to a substantial zonal mean despite the local X being smaller in magnitude than those when using the rL scheme. In JJA, we see mixing at 122 hPa over the Maritime Continent (around 120°E). This region has a very background low wind shear, and so the mixing in this region does not result in a large zonal acceleration.

3. Modeling the response to forcing terms

We have shown that substantial forcing terms Q and X can arise from vertical mixing, but that these terms are dependent on and very sensitive to the mixing scheme. Therefore, it is important to understand the order of magnitude of the response to these forcing terms as a measure of the level of uncertainty associated with the representation of vertical mixing in a model. In this section, we shall model the response to idealized forcings with similar structures to the observed climatology of forcing terms arising from the revised Louis scheme shown in Figure 4.

a. Model

We use the Geophysical Fluid Dynamics Laboratory (GFDL) Flexible Modeling System (FMS) spectral dynamical core running at T42 resolution (i.e. approximately 2.8° by 2.8°). Newtonian cooling and Rayleigh damping are applied as specified in Held and Suarez (1994, henceforth referred to as HS94). The equilibrium temperature profile is also that specified in HS94. The Newtonian cooling timescale in the upper troposphere and lower stratosphere is 40 days.

We use 60 vertical levels with approximately 800 m resolution in the TTL and lower stratosphere. The vertical levels are distributed

$$\sigma_i = \exp\left[5.5\left(\frac{i}{n} + \left(\frac{i}{n}\right)^3\right)\right],$$

where σ_i is the i^{th} level in σ-coordinates, (i.e. the pressure on level i is given by $p_i = p_{\text{surf}}\sigma_i$ where p_{surf} is the instantaneous surface pressure), and n is the total number of levels. Here, $n = 60$. The model top is at 11 scale heights with a sponge layer above 1 hPa.

b. *Imposed Diabatic Forcings*

We shall impose idealized forcings (both temperature tendency and zonal acceleration) with similar structures to those observed in section 2, focusing on the dipole structure observed in the zonal mean forcing due to mixing (Figure 1), and on the dipole structure observed in the Indian Ocean region (shown in Figure 4). We use an idealized zonally symmetric forcing of the form

$$F^{\text{sym}} = \begin{cases} A\cos\left(\frac{\pi y}{2L_{\text{y}}}\right)\sin\left(\frac{\pi(z_0 - z)}{L_{\text{z}}}\right) & \text{where } |y| < L_{\text{y}}, |z| < L_{\text{z}}, \\ 0 & \text{otherwise,} \end{cases} \tag{2}$$

to represent the dipole structure in the zonal mean, where L_{y} and L_{z} are the half-widths in the meridional and vertical directions. z is log-pressure height, and z_0 is the log-pressure height about which the forcing is located. We choose these parameters such that the forcing resembles the dipole structure observed in the zonal mean (Figure 1), with $L_{\text{y}} = 10°$ latitude ≈ 1100 km, $L_{\text{z}} = 0.5$ scale heights ≈ 3.5 km and $z_0 = 2.2$ scale heights ≈ 15.5 km $\approx$ 110 hPa. A is the amplitude of the forcing, and will be specified later.

We use an idealized forcing of the form

$$F = \begin{cases} \frac{\pi^2 a}{2L_{\text{x}}}\cos\left(\frac{\pi x}{2L_{\text{x}}}\right)F^{\text{sym}} & \text{where } |x| < L_{\text{x}}, \\ 0 & \text{otherwise,} \end{cases} \tag{3}$$

to represent the localized dipole structure in the JJA Indian Ocean, where L_{x} is the half-width in the zonal direction, and a is the radius of the Earth. We choose $L_{\text{x}} = 30°$ longitude

≈ 3300 km, with the remaining parameters specified as in Eq. (2). The zonal structure of Eq. (3) is such that $F^{\text{sym}} = \overline{F}$ (where $\bar{\cdot}$ denotes the zonal mean.)

We define a local temperature tendency forcing F_Q that has the structure given in Eq. (3) and a zonal mean amplitude $A = 0.1\ \mathrm{K\,day^{-1}}$ (chosen to give a similar 10°N–10°S average zonal mean amplitude of approximately $0.06\ \mathrm{K\,day^{-1}}$ as that in ERA-Interim in JJA shown in Figure 1). We also define a local zonal acceleration forcing F_X with the same structure and with $A = 0.3\ \mathrm{m\,s^{-1}\,day^{-1}}$ (again, chosen to give a similar amplitude of approximately $0.2\ \mathrm{K\,day^{-1}}$ to that in ERA-Interim in JJA shown in Figure 1). The zonally symmetric forcings are defined as F_Q^{sym} and F_X^{sym}.

We compute an 8000 day control run with no imposed forcing (i.e. with just the HS94 Newtonian cooling and Rayleigh friction). For each forcing, a forced run is then initialized from the end of the control run, and is again integrated for 8000 days. We define the control climate to be the average of the last 4000 days of the control run, and the forced climate to be the average of the last 4000 days of the forced run. We denote the climatological average over the last 4000 days of each run by $\langle\cdot\rangle$. The last 4000 days of the unforced control run will be denoted by (T_0, u_0, v_0, w_0) and the last 4000 days of each forced run will be denoted by (T_1, u_1, v_1, w_1). The climate perturbation δ to the unforced climate is then defined as

$$\delta x = \langle x_1 \rangle - \langle x_0 \rangle \,, \tag{4}$$

where x is some model variable or derived quantity, such as temperature.

c. *Zonal Mean Response to the Imposed Forcings*

We shall first present the zonal mean response to the zonally symmetric forcings F_X^{sym} and F_Q^{sym}, and to the localized forcings F_X and F_Q. Figure 6 shows the zonal mean temperature response $\delta\overline{T}$ and zonal wind response $\delta\overline{u}$ averaged over 10°N–10°S latitude (referred to here the inner tropical zonal mean response) to F_X^{sym}, F_Q^{sym}, and both F_X^{sym} and F_Q^{sym} together. We see that the inner tropical zonal mean temperature response has a dipole structure similar to the dipole forcing structure for all forcings. Figure 6 also shows the inner tropical zonal mean response to the equivalent localized forcings F_X, F_Q, and both F_X and F_Q together. We see that the zonal mean inner tropical responses to the localized forcings are very similar to the equivalent responses to the zonally symmetric forcings, which demonstrates that the localized solutions are fairly linear. The exception to this similarity is the inner tropical zonal mean wind response to F_Q and F_Q^{sym}, which show substantial differences above the 100 hPa level, which will be discussed in more detail below.

We define the magnitude of the inner tropical zonal mean response as the maximum of the absolute value of the inner tropical zonal mean response over levels between 130 hPa and 60 hPa. Table 1 summarizes the magnitudes of the responses shown in Figure 6. Again, we note that the zonally symmetric forcing gives a very similar magnitude response to the zonally localized forcings. We also see that the temperature response to both forcings is similar to the sum of the responses to each forcing. Again, this indicates that the responses are fairly linear. Both the temperature and wind responses are dominated by the response to F_X, which is responsible for approximately 65% of the temperature response to both forcings and for almost all of the zonal wind response. The combined forcings yield a response of approximately 3.5 K, which is highly significant in the context of tropical tropopause temperatures and stratospheric water vapor.

Figure 7 shows $\delta\overline{T}$ and $\delta\overline{u}$ for all of the forcings above. As above, the responses to the symmetric forcing and the equivalent localized forcing are very similar, and the response to $F_X$is larger than the response to F_Q, with the response to both forcings dominated by the response to F_X. We see that the responses to F_X and F_X^{sym} are largest in the inner tropics (10°N–10°S where the forcing is largest) but we see a wider response in the lower stratosphere, with the cold anomaly at 70 hPa extending to approximately 20° latitude. The dipole structure in the response is at a slightly higher altitude than the forcing, and the cold anomaly extends above the forced region. There is also a response in the upper troposphere that is strongest at 30° latitude. This tropospheric response is very similar to that shown in

Garfinkel and Hartmann (2011).

The responses to F_Q and F_Q^{sym} shown in Figure 7 (panels b and e) have a wider latitudinal structure than the responses to F_X and F_X^{sym}, extending to approximately 15°. The zonal wind responses to F_Q and F_Q^{sym} are quite different, with an order 4 $\mathrm{m\,s^{-1}}$ zonal wind response to F_Q, but little response to F_Q^{sym}.

d. Zonally Asymmetric Response to Localized Forcings

Figure 8 shows the zonally asymmetric response to local forcings F_X, F_Q, and both F_X and F_Q in the inner tropics (10°N–10°S). We see that both responses are quite zonally symmetric, and as such we do not emphasize the zonally asymmetric structure of the response to localized forcings in this paper, and will only describe the structure briefly.

The response to F_X is particularly zonally symmetric, with strong winds of up to 12 $\mathrm{m\,s^{-1}}$ at around 100 hPa. Winds are strongest in the forced region. The thermal wind temperature response has more asymmetry (due to changing latitudinal structure, not shown here). The response to F_Q is less symmetric, and resembles a stationary Kelvin wave. Given appropriate easterly zonal winds in the TTL, the imposed forcing can excite a stationary Kelvin wave (one that propagates at the same speed as the background wind, and so is stationary when Doppler shifted) if the vertical structure of the forcing is close to the stationary Kelvin wave vertical structure. This stationary wave propagates vertically from the forced region into the stratosphere, and decelerates the stratosphere at around 50 hPa in Figure 8b. The stationary wave accelerates the forced region, and is therefore also responsible for the westerly wind response to F_X from 100 hPa to 50 hPa in Figures 6 and 7e. The response to both F_X and F_Q shown in Figure 8c is close to the linear superposition of the two solutions. Most of the zonal asymmetry comes from the response to F_Q, leading to the strongest wind responses away from the forced region.

4. Interpretation of Results

In the following, we will focus on the zonally symmetric cases F_Q^{sym} and F_X^{sym} since the asymmetric forcings give similar responses in the zonal mean (see section 3) and give very similar results in the analysis presented below (not shown). In order to investigate the responses to the zonally symmetric forcings, we analyze the time mean zonal mean momentum and buoyancy equations.

a. Response to Imposed Heating

The imposed heating F_Q^{sym} forces the time mean zonal mean buoyancy equation (Andrews et al. 1987, p124),

$$\frac{\partial\overline{\theta}}{\partial t}+a^{-1}\overline{v}\frac{\partial\overline{\theta}}{\partial\phi}+\overline{w}\frac{\partial\overline{\theta}}{\partial z}=-\tau^{-1}(\overline{\theta}-\theta_{eq})+e^{\kappa z/H}F_Q^{\mathrm{sym}}-\frac{1}{a\cos\phi}\frac{\partial(\overline{\theta' v'}\cos\phi)}{\partial\phi}-\frac{1}{\rho_0}\frac{\partial(\rho_0\overline{\theta' w'})}{\partial z}, \quad (5)$$

where $\kappa = R/c_p$, ϕ is latitude, τ is the Newtonian cooling timescale (40 days in this study), θ is the potential temperature, ρ_0 is the log-pressure density and a is the Earth's radius. The $\partial\overline{\theta}/\partial t$ term disappears when we take the climatological mean. The climatological means of the remaining terms (computed offline) averaged over $\pm10°$ latitude are shown in Figure 9a. The budget is not perfectly closed due to the offline nature of the calculation, but the errors are small. We see that the vertical advection term and the Newtonian cooling term are the dominant balance.

Figure 9b shows the difference between the unforced and forced runs in these terms. We see that

$$\delta\left(\overline{w}\frac{\partial\overline{\theta}}{\partial z}\right)+\tau^{-1}\delta\overline{\theta}\approx e^{\kappa z/H}F_Q^{\mathrm{sym}}, \quad (6)$$

with both of these terms of a similar order of magnitude. All of the remaining terms do not significantly change from the unforced run to the forced run and so do not contribute to the response.

As noted in section 3, the responses to F_X^{sym} and F_Q^{sym} are approximately linear. Therefore, we write the change in vertical advection in terms of the base climatology and the change in the climatology, as

$$\delta\left(\overline{w}\frac{\partial\overline{\theta}}{\partial z}\right) = \langle\overline{w_0}\rangle\frac{\partial\delta\overline{\theta}}{\partial z} + \delta\overline{w}\frac{\partial\langle\overline{\theta_0}\rangle}{\partial z} + \delta\overline{w}\frac{\partial\delta\overline{\theta}}{\partial z}.$$

The first of these linear terms is dominant (except below 140 hPa, where the second term is of a similar order of magnitude to the first term), so

$$\left(\langle\overline{w_0}\rangle\frac{\partial}{\partial z} + \tau^{-1}\right)\delta\overline{\theta} \approx e^{\kappa z/H} F_Q^{\mathrm{sym}}. \tag{7}$$

Therefore, as a parcel rises due to the climatological upwelling $\langle\overline{w_0}\rangle$ it is warmed by the positive region of F_Q^{sym}, cools radiatively, then is further cooled by the negative region of F_Q^{sym} before returning to the unforced solution above the forcing region by radiative heating. This explains the phase lag in the vertical between the forcing structure and the temperature response that can be seen in Figure 9b. Eq. (7) shows that either increasing the climatological upwelling $\langle\overline{w_0}\rangle$ or reducing the Newtonian cooling timescale τ would lead to a reduction in the temperature amplitude of the response to F_Q^{sym}.

The zonal wind response to F_Q^{sym} is in thermal wind balance with the temperature response, so using the thermal wind equation near the equator (given by Andrews et al. 1987, p318),

$$\frac{\partial\delta\overline{u}}{\partial z} \approx -\frac{R}{H\beta a^2}\frac{\partial^2\delta\overline{T}}{\partial\phi^2}. \tag{8}$$

b. *Response to Imposed Zonal Acceleration*

We use a similar analysis here as was used above for the response to the imposed heating, but analyzing the zonal mean zonal momentum equation (Andrews et al. 1987, p124),

$$\frac{\partial\overline{u}}{\partial t} + \overline{v}\left[\frac{1}{a\cos\phi}\frac{\partial(\overline{u}\cos\phi)}{\partial\phi} - f\right] + \overline{w}\frac{\partial\overline{u}}{\partial z} = F_X^{\mathrm{sym}} - \frac{1}{a\cos^2\phi}\frac{\partial(\overline{u'v'}\cos^2\phi)}{\partial\phi} - \frac{1}{\rho_0}\frac{\partial(\rho_0\overline{u'w'})}{\partial z}. \tag{9}$$

Again, the $\partial\overline{u}/\partial t$ term disappears when we compute the climatological mean of this equation, and we show the climatological means of the remaining terms in Figure 10a. The zonal momentum budget is less straightforward than the heat budget above as all the terms have similar orders of magnitude. However, when we compute the difference between the forced and unforced runs (Figure 10b) we see that the only term to significantly change is the vertical advection term, so

$$\delta\left(\overline{w}\frac{\partial\overline{u}}{\partial z}\right) \approx F_X^{\mathrm{sym}}.$$

Shaw and Boos (2012) force a dry GCM with a localized zonal acceleration forcing in the upper troposphere and also find that the vertical advection term is important (they discuss the equivalent term in the vorticity equation).

As above, we can write the change in vertical advection in terms of the base climatology and the change in the climatology, as

$$\delta\left(\overline{w}\frac{\partial\overline{u}}{\partial z}\right) = \langle\overline{w_0}\rangle\frac{\partial\delta\overline{u}}{\partial z} + \delta\overline{w}\frac{\partial\langle\overline{u_0}\rangle}{\partial z} + \delta\overline{w}\frac{\partial\delta\overline{u}}{\partial z}.$$

The first of these linear terms is dominant, so

$$\langle\overline{w_0}\rangle\frac{\partial\delta\overline{u}}{\partial z} \approx F_X^{\mathrm{sym}}. \tag{10}$$

The zonal wind response to F_X^{sym} can therefore be explained by considering a parcel of air rising due to the climatological upwelling $\langle\overline{w_0}\rangle$ that is first accelerated by the positive region of $F_X^{\mathrm{sym}}$and is then decelerated by the negative region of F_X^{sym}. This explains the single-signed form of the zonal wind response to the dipole forcing. From Eq. (10), we see that an increase in climatological vertical wind $\langle w_0\rangle$ would reduce the amplitude of the response $\delta\overline{u}$ to F_X^{sym}, with $\delta\overline{u} \sim \langle\overline{w_0}\rangle^{-1}$.

5. Conclusions

We have calculated the diabatic heating and zonal acceleration due to mixing based on two parametrisations of shear-flow mixing. We find a substantial heating and acceleration in the TTL. These forcing terms take a dipole structure confined to the inner tropics, and are strongest in boreal summer over the Indian Ocean. The climatological heating and acceleration terms in ERA-Interim are largest in boreal summer over the Indian Ocean, with amplitudes of 0.5 $\mathrm{K\,day^{-1}}$ and 2 $\mathrm{m\,s^{-1}\,day^{-1}}$ respectively. In the zonal mean averaged over the inner tropics, the magnitude of the heating and acceleration terms are 0.08 $\mathrm{K\,day^{-1}}$ and 0.2 $\mathrm{m\,s^{-1}\,day^{-1}}$. We have used a dry dynamical core to calculate the response to forcings similar to those found in the climatology of ERA-Interim, and find remarkably large responses in temperature and zonal wind. Forcings of a similar magnitude to those found in ERA-Interim during JJA produce a 4 K temperature response and a 12 $\mathrm{m\,s^{-1}}$ zonal wind response in the TTL. Such a temperature response would have a large effect on water vapor entering the stratosphere, changing TTL water vapor concentration by approximately 2 ppmv (roughly 75% of the current mixing ratio for air entering the lower stratosphere; Fueglistaler and Haynes 2005).

Further, we find that the amplitude of the response is dependent on the mean upwelling $\langle\overline{w_0}\rangle$, and that the amplitude of the response to heating (a comparatively small proportion of the response to both heating and forcing; see section 2) is also dependent on the radiative timescale τ. We therefore compare $\langle\overline{w_0}\rangle$ and τ between the background climatology of the dry GCM and ERA-Interim to assess whether the response is likely to be similar for a realistic base state.

Figure 11 shows the climatology of $\overline{w}$ in ERA-Interim, along with the upwelling $\langle\overline{w_0}\rangle$ from the background model run. We see that below the 100 hPa level, the model upwelling is approximately 2 to 3 times smaller than the annual mean upwelling in ERA-Interim, but above the 100 hPa level, model upwelling is similar to the annual mean upwelling in ERA-Interim. Dee et al. (2011) note that the mean vertical transport velocity in ERA-Interim is greater than water vapor observations suggest (Schoeberl et al. 2008) in the lower stratosphere, so model upwelling $\langle\overline{w_0}\rangle$ may be larger than in reality above the 100 hPa level. We can therefore conclude that the response to the forcing with a more realistic basic state is likely to be smaller below the 100 hPa level, but similar or possibly larger above the 100 hPa level.

Upwelling in ERA-Interim has a clear annual cycle, with a minimum in upwelling at

100 hPa in September, and a maximum upwelling at 100 hPa in boreal winter, in agreement with Randel et al. (2007). The minimum upwelling in ERA-Interim in JJA coincides with the largest forcing from the mixing scheme (both locally over the Indian Ocean and also in the zonal mean; see Figures 1 and 2), potentially amplifying the response to mixing in the summer, and suppressing the response to mixing in the winter, leading to a large annual cycle in the response to mixing. This relationship would be interesting to investigate in a future study.

The τ used in the model here (as specified in HS94) is 40 days. We have used the Fu and Liou (1992) radiation scheme with perturbations of a similar vertical scale to the responses shown in section 3, and find that τ varies with height, is approximately 15 days at 100 hPa, and decreases with height into the stratosphere (not shown). This indicates that the τ used in the model in this study is too long, and that the true response to the forcing should be smaller. In section 4 we showed that τ only affects the amplitude of the response to the imposed heating, and this is the smaller component of the response to both forcings. Therefore, we expect that changing τ would have only a small affect on the overall response.

Taking the corrections mentioned above into account, we would expect that the response to vertical mixing in ERA-Interim and similar models to be order 2 K to 4 K, and order 6 $\mathrm{m\,s^{-1}}$ to 12 $\mathrm{m\,s^{-1}}$ in the boreal summer. This is a substantial response in the context of TTL temperatures and winds.

The modeling study presented here uses a steady state forcing that has a similar average structure to the forcing in ERA-Interim during JJA. In reality, the forcing strongly varies with time and is very intermittent (see Flannaghan and Fueglistaler (2011)). However, the model's response to the forcing is quite linear. Consequently, we do not expect that this simplification substantially alters the nature of the solution. Similarly, we have not investigated the solution to a slowly varying annual cycle in forcing. The timescales of the solution are the advection timescale and the Newtonian cooling timescale. The timescale for vertical advection in reality is of order 2 to 3 months (Fueglistaler et al. 2009a). As noted above, there is an annual cycle in $\overline{w}$, and therefore there is also some seasonal variation in the advection timescale. The timescale of Newtonian cooling τ is set as $\tau = 40$ days, whereas in reality a reasonable estimate is $\tau \approx 15$ days. Clearly the Newtonian cooling timescale is shorter than the interseasonal variability in the forcing terms and so would not be expected to be important for interseasonal variability. The advection timescale however is sufficiently long to suggest that interseasonal variability would significantly affect the solution. To investigate the effect of interseasonal variability further, a model with more reasonable upwelling velocities (and annual cycle in upwelling) would be needed, and so is beyond the scope of this study. However, investigating the effect of interseasonal variability of the background state is an important study to perform as it could significantly alter the magnitude and seasonality of the response.

Mixing schemes are a modeling detail that are not often discussed with respect to studies of the TTL, and are sometimes used as tuning parameters. We have shown that these mixing schemes have the potential to produce significant impacts on the climate of the model, highlighting the particular importance of mixing schemes to TTL winds and temperatures in climate models. Mixing has been observed to occur in the TTL and can be very intense (Fujiwara et al. 1998; Fujiwara and Takahashi 2001; Fujiwara et al. 2003), and so it is possible that mixing could have a significant effect the climate of the TTL in reality.

Acknowledgments.

This research was supported by DOE grant SC0006841. We thank the Geophysical Fluid Dynamics Laboratory for providing the model used in this study and for providing the computer time to perform the model runs. We thank ECMWF for providing the ERA-Interim data.

APPENDIX

Mixing scheme definitions

Parametrisation schemes typically approximate mixing as a diffusive process, with the diabatic tendency due to mixing given by

$$\rho \left(\frac{\partial \phi}{\partial t} \right)_{\text{mix}} = \frac{\partial}{\partial z} \left(\rho K_\phi \frac{\partial \phi}{\partial z} \right), \tag{A1}$$

where ϕ is the quantity being mixed (dry static energy when computing heat fluxes and temperature tendency or horizontal wind when computing momentum fluxes and acceleration), and K_ϕ is the exchange coefficient.

The parametrisation defines K_ϕ in terms of the bulk (grid-scale) quantities, and here is defined as

$$K_\phi = \ell^2 \left| \frac{\partial \mathbf{u}}{\partial z} \right| f_\phi(Ri). \tag{A2}$$

Here, ℓ is the nominal mixing length, and dimensionalizes the equation.

a. Monin-Obukhov-motivated (MO) scheme

The ECMWF IFS has, since Cycle 33 (IFS Cy33r1), used a scheme that is inspired by the solution given by Monin and Obukhov (1954) to the problem of boundary layer turbulence, but is applied throughout the free atmosphere (Nieuwstadt 1984). This scheme is qualitatively similar to the scheme used in the NCAR CAM4 model (Bretherton and Park 2009).

In statically stable conditions, where $Ri > 0$, the exchange coefficients K_M and K_H for momentum and heat are defined by Eq. (A2) with

$$f_\mathrm{M}(Ri) = (1 + 5\zeta)^{-2}, \tag{A3a}$$

$$f_\mathrm{H}(Ri) = \frac{1}{(1 + 5\zeta)(1 + 4\zeta)^2}, \tag{A3b}$$

where ζ is a non-dimensional function of Ri, defined as the solution to

$$Ri = \frac{\zeta(0.74 + 4.7\zeta)}{(1 + 4.7\zeta)^2}, \tag{A4}$$

which is a fit to observational data given in Businger et al. (1971). When $Ri < 0$ (statically unstable conditions),

$$f_{\mathrm{M}}(Ri) = (1 - 16Ri)^{1/2}, \tag{A5a}$$

$$f_{\mathrm{H}}(Ri) = (1 - 16Ri)^{3/4}. \tag{A5b}$$

The nominal mixing length, ℓ, is set at a constant value of 150 m in the MO scheme. Figure 12 shows f_{M} and f_{H} as a function of Richardson number Ri as defined in this section.

Eq. (A3) and Eq. (A5) are taken from the ECMWF IFS Cy33r1 documentation, and Eq. (A3) is very similar to the equivalent relation given by Businger et al. (1971), although not exactly the same. In the ECMWF IFS Cy33r1 documentation, the definition of ζ is not given, and so the definition of ζ given by Eq. (A4) is taken from Businger et al. (1971). We expect the equivalent relation in the IFS parametrisation to be similar.

b. Revised Louis (rL) scheme

The ECMWF IFS model prior to Cycle 33, including the version used in the ECMWF ERA-Interim project (IFS Cy31r2) (Dee et al. 2011), uses a different scheme, which was originally devised to be numerically simple to compute, but is used in IFS Cy31r2 because it increases the amount of mixing in the lower troposphere, which was absent when using the MO scheme. The scheme used is a revised version of the Louis scheme (Louis 1979), and is given as

$$f_{\mathrm{M}}(Ri) = \frac{1}{1 + 10Ri(1 + Ri)^{-1/2}}, \tag{A6a}$$

$$f_{\mathrm{H}}(Ri) = \frac{1}{1 + 10Ri(1 + Ri)^{1/2}}, \tag{A6b}$$

when $Ri > 0$. When $Ri < 0$, f_{M} and f_{H} are the same as given above for the MO scheme in Eq. (A5).

The nominal mixing length ℓ is approximately 40 m in the rL scheme. Here, ℓ depends on height, but over the TTL it is approximately constant, and for this study it is sufficient to use a value of 40 m.

Figure 12 shows f_M and f_H for both the MO and rL schemes. We see that the rL scheme has a long tail, with significant mixing occurring even at $Ri \sim 1$. The long tail of the rL scheme contributes a lot of additional mixing compared with the MO scheme. However, $\ell \approx 40$ m in the TTL in the rL scheme but $\ell = 150$ m in the MO scheme, resulting in similar average exchange coefficients for both schemes. Other mixing schemes, such as the scheme used in NCAR CAM3, are qualitatively similar to the rL scheme, with no cut-off in Richardson number (Bretherton and Park 2009).

Validation of Offline Scheme

ERA-Interim provides a total diabatic heating output, and a total radiative heating output (including the radiative contribution from clouds). The difference of these two fields, the residual diabatic temperature tendency, gives the contribution from all non-radiative diabatic processes, which are predominantly latent heating and mixing, shown by Fueglistaler et al. (2009b). Unfortunately these are not available separately. To test the validity of applying the mixing scheme offline, we compare the residual diabatic temperature tendency in ERA-Interim with the temperature tendency predicted by the offline mixing scheme.

Figure 13 shows the zonal mean ECMWF residual diabatic temperature tendency, the temperature tendency predicted by the offline mixing scheme, and the difference between these two quantities averaged over 1 January 2000 to 20 January 2000 averaged over 10°N to 10°S. In all results presented here, the mixing scheme is applied to the data before any averaging takes place. This is essential as the mixing schemes are highly non-linear. We see that below the 100 hPa level, there is a large positive temperature tendency in the ERA-Interim residual that is not captured by the mixing scheme. This is due to convection and the associated latent heat release. Above the 100 hPa level, the residual is slightly more negative than that predicted by the mixing scheme; this is due to convective cold tops. In regions of no convection, the offline mixing calculation fits the residual term very well, with errors of approximately 10% throughout the TTL (Flannaghan and Fueglistaler 2011), and so we conclude that the offline application of the mixing scheme can be expected to give a fair representation of the model vertical mixing throughout the TTL.

REFERENCES

Andrews, D., J. Holton, and C. Leovy, 1987: *Middle atmosphere dynamics*, Vol. 40. Academic Pr, URL `http://books.google.co.uk/books?hl=en\&lr=\&id=N1oNurYZefAC\&oi=fnd\&pg=PR9\&dq=middle+atmosphere+dynamics\&ots=Pzqs67yIjJ\&sig=zOBp\_-hnWfAhycb6BEGRA5H3-ag`.

Bretherton, C. S. and S. Park, 2009: A New Moist Turbulence Parameterization in the Community Atmosphere Model. *Journal of Climate*, **22 (12)**, 3422–3448, doi:10.1175/2008JCLI2556.1, URL `http://journals.ametsoc.org/doi/pdf/10.1175/2008JCLI2556.1http://journals.ametsoc.org/doi/abs/10.1175/2008JCLI2556.1`.

Businger, J. A., J. C. Wyngaard, Y. Izumi, and E. F. Bradley, 1971: Flux-Profile Relationships in the Atmospheric Surface Layer. *Journal of the Atmospheric Sciences*, **28 (2)**, 181–189, doi:10.1175/1520-0469(1971)028⟨0181:FPRITA⟩2.0.CO;2, URL `http://www.iag.usp.br/meteo/labmicro/cursos/pos-graduacao/Businger\_etal\_1971\_FLUX\_PROFILE\_RELANTIONSHIPS\_IN\_THE\_ATMOSPHERIC\_SURFACE\_LAYER.pdfhttp://journals.ametsoc.org/doi/abs/10.1175/1520-0469\%281971\%29028\%3C0181\%3AFPRITA\%3E2.0.CO\%3B2`.

Dee, D. P., et al., 2011: The ERA-Interim reanalysis: configuration and performance of the data assimilation system. *Quarterly Journal of the Royal Meteorological Society*, **137 (656)**, 553–597, doi:10.1002/qj.828, URL `http://doi.wiley.com/10.1002/qj.828`.

Flannaghan, T. J. and S. Fueglistaler, 2011: Kelvin waves and shear-flow turbulent mixing in the TTL in (re-)analysis data. *Geophysical Research Letters*, **38**, L02 801, doi:10.1029/2010GL045524, URL `http://www.agu.org/pubs/crossref/2011/2010GL045524.shtml`.

Fu, Q. and K. Liou, 1992: On the correlated k-distribution method for radiative transfer in nonhomogeneous atmospheres. *Journal of the Atmospheric Sciences*, **49 (22)**, 2139–2156, URL http://irina.eas.gatech.edu/EAS8803_Fall2007/Fu_Liou1992.pdf.

Fueglistaler, S., A. E. Dessler, T. J. Dunkerton, I. Folkins, Q. Fu, and P. W. Mote, 2009a: Tropical tropopause layer. *Reviews of Geophysics*, **47 (1)**, RG1004, doi:10.1029/2008RG000267, URL http://www.mathstat.dal.ca/~folkins/TTL-review-RG.pdfhttp://www.agu.org/pubs/crossref/2009/2008RG000267.shtml.

Fueglistaler, S. and P. H. Haynes, 2005: Control of interannual and longer-term variability of stratospheric water vapor. *Journal of Geophysical Research*, **110 (D24)**, D24 108, doi:10.1029/2005JD006019, URL http://doi.wiley.com/10.1029/2005JD006019.

Fueglistaler, S., B. Legras, A. Beljaars, J. Morcrette, A. Simmons, A. Tompkins, and S. Uppala, 2009b: The diabatic heat budget of the upper troposphere and lower/mid stratosphere in ECMWF reanalyses. *Quarterly Journal of the Royal Meteorological Society*, **135 (638)**, 21–37, doi:10.1002/qj, URL http://onlinelibrary.wiley.com/doi/10.1002/qj.361/abstract.

Fujiwara, M., K. Kita, and T. Ogawa, 1998: Stratosphere-troposphere exchange of ozone associated with the equatorial Kelvin wave as observed with ozonesondes and rawinsondes. *Journal of Geophysical Research*, **103 (D15)**, 19 173–19 182, doi:10.1029/98JD01419, URL http://www.agu.org/pubs/crossref/1998/98JD01419.shtml.

Fujiwara, M. and M. Takahashi, 2001: Role of the equatorial Kelvin wave in stratosphere-troposphere exchange in a general circulation model. *Journal of Geophysical Research*, **106 (D19)**, 22 763–22 780, doi:10.1029/2000JD000161, URL http://www.agu.org/pubs/crossref/2001/2000JD000161.shtml.

Fujiwara, M., M. K. Yamamoto, H. Hashiguchi, T. Horinouchi, and S. Fukao, 2003: Turbulence at the tropopause due to breaking Kelvin waves observed by the

Equatorial Atmosphere Radar. *Geophysical Research Letters*, **30 (4)**, 1171, doi:10.1029/2002GL016278, URL http://www.agu.org/pubs/crossref/2003/2002GL016278.shtmlhttp://doi.wiley.com/10.1029/2002GL016278.

Garfinkel, C. I. and D. L. Hartmann, 2011: The Influence of the Quasi-Biennial Oscillation on the Troposphere in Winter in a Hierarchy of Models. Part I: Simplified Dry GCMs. *Journal of the Atmospheric Sciences*, **68 (6)**, 1273–1289, doi:10.1175/2011JAS3665.1, URL http://journals.ametsoc.org/doi/abs/10.1175/2011JAS3665.1.

Held, I. M. and M. J. Suarez, 1994: A Proposal for the Intercomparison of the Dynamical Cores of Atmospheric General Circulation Models. *Bulletin of the American Meteorological Society*, **75 (10)**, 1825–1830, doi:10.1175/1520-0477(1994)075⟨1825:APFTIO⟩2.0.CO;2, URL http://www.gfdl.gov/bibliography/related_files/ih9401.pdfhttp://journals.ametsoc.org/doi/abs/10.1175/1520-0477\%281994\%29075\%3C1825\%3AAPFTIO\%3E2.0.CO\%3B2.

Louis, J., 1979: A parametric model of vertical eddy fluxes in the atmosphere. *Boundary-Layer Meteorology*, **7**, 187–202, URL http://www.springerlink.com/index/h4440726140826j5.pdf.

Monin, A. and A. Obukhov, 1954: Basic laws of turbulent mixing in the surface layer of the atmosphere. *Trudy Geofiz. Inst. Acad. Nauk SSSR*, URL http://gronourson.free.fr/IRSN/Balagan/Monin_and_Obukhov_1954.pdf.

Nieuwstadt, F., 1984: The turbulent structure of the stable, nocturnal boundary layer. *Journal of the Atmospheric Sciences*, **41 (14)**, 2202–2216, URL http://cat.inist.fr/?aModele=afficheN\&cpsidt=9092550.

Randel, W. J., M. Park, F. Wu, and N. Livesey, 2007: A Large Annual Cycle in Ozone above the Tropical Tropopause Linked to the BrewerDobson Circulation. *Journal of the

Atmospheric Sciences, **64 (12)**, 4479–4488, doi:10.1175/2007JAS2409.1, URL http://journals.ametsoc.org/doi/abs/10.1175/2007JAS2409.1.

Schoeberl, M. R., a. R. Douglass, R. S. Stolarski, S. Pawson, S. E. Strahan, and W. Read, 2008: Comparison of lower stratospheric tropical mean vertical velocities. *Journal of Geophysical Research*, **113 (D24)**, D24 109, doi:10.1029/2008JD010221, URL http://doi.wiley.com/10.1029/2008JD010221.

Shaw, T. A. and W. R. Boos, 2012: The Tropospheric Response to Tropical and Subtropical Zonally Asymmetric Torques: Analytical and Idealized Numerical Model Results. *Journal of the Atmospheric Sciences*, **69 (1)**, 214–235, doi:10.1175/JAS-D-11-0139.1, URL http://journals.ametsoc.org/doi/abs/10.1175/JAS-D-11-0139.1.

Simmons, A., S. Uppala, D. Dee, and S. Kobayashi, 2007: ERA-Interim: New ECMWF reanalysis products from 1989 onwards. *ECMWF Newsletter*, **(110)**, 25–35.

Viterbo, P., A. Beljaars, J. Mahfouf, and J. Teixeira, 1999: The representation of soil moisture freezing and its impact on the stable boundary layer. *Quarterly Journal of the Royal Meteorological Society*, **125 (559)**, 2401–2426, URL http://onlinelibrary.wiley.com/doi/10.1002/qj.49712555904/abstract.

Wright, J. S. and S. Fueglistaler, 2013: Large differences in reanalyses of diabatic heating in the tropical upper troposphere and lower stratosphere. *Atmospheric Chemistry and Physics*, **13 (18)**, 9565–9576, doi:10.5194/acp-13-9565-2013, URL http://www.atmos-chem-phys-discuss.net/13/8805/2013/http://www.atmos-chem-phys.net/13/9565/2013/.

List of Tables

	Symmetric forcing		Localized forcing	
Forcing type	Temp, K	Wind, $\mathrm{m\,s^{-1}}$	Temp, K	Wind, $\mathrm{m\,s^{-1}}$
F_X	2.8	11.9	2.5	12.1
F_Q	1.4	1.3	1.3	3.2
F_X and F_Q	3.3	11.9	3.7	12.7

TABLE 1. The magnitude of the inner tropical zonal mean response to zonally symmetric forcing and zonally localized forcing. The magnitude of the inner tropical zonal mean response is defined as the maximum of the absolute value of the inner tropical zonal mean response over levels between 130 hPa and 60 hPa.

List of Figures

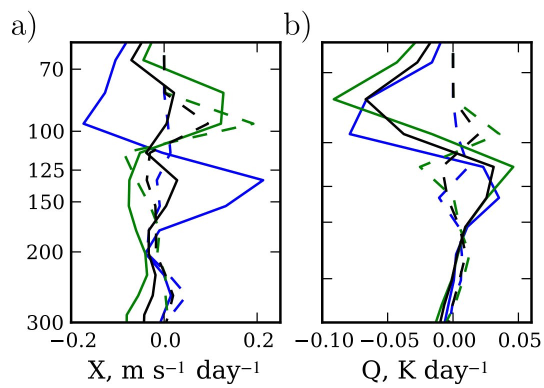

Fig. 1. Climatological mean profiles (1989–2009) averaged over 10°N–10°S of a) Zonal mean zonal acceleration, $\overline{X}$, and b) zonal mean temperature tendency, $\overline{Q}$, for DJF (green), JJA (blue) and the annual average (black). Diabatic terms are computed using the rL scheme (solid) and the MO scheme (dashed).

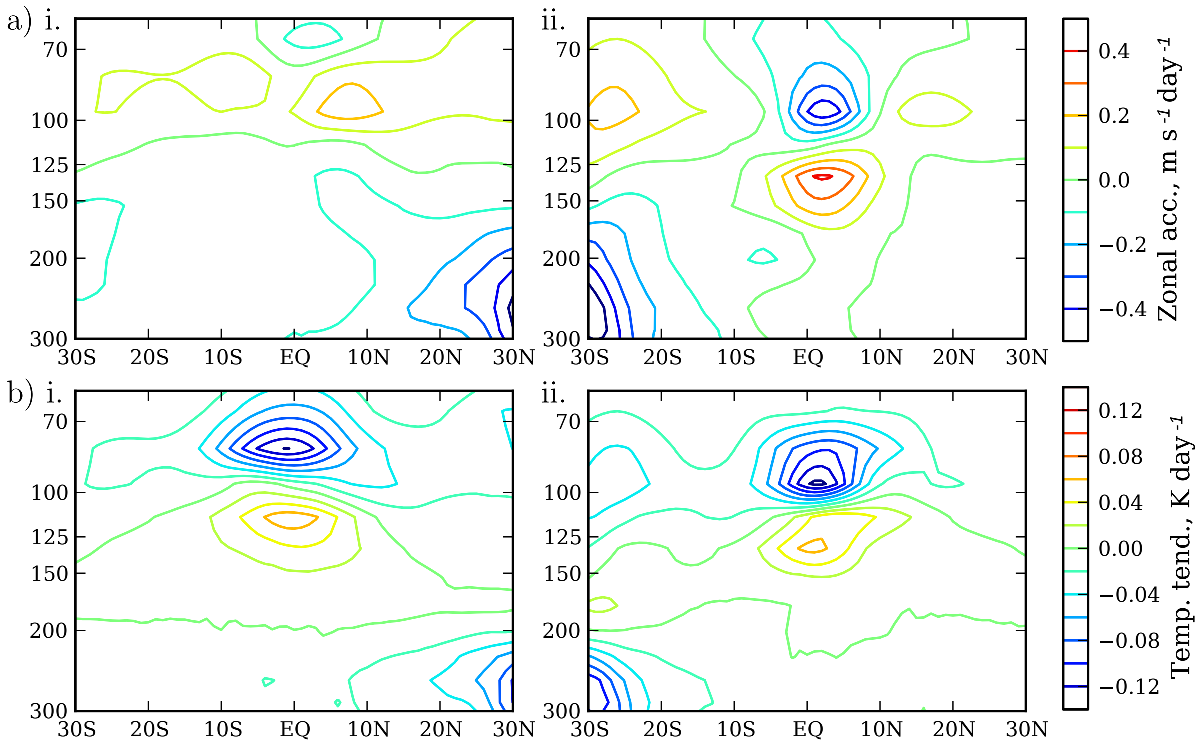

Fig. 2. Climatological zonal mean a) zonal acceleration and b) temperature tendency for i) DJF and ii) JJA computed using the rL scheme applied to ERA-Interim data from 1989 to 2009.

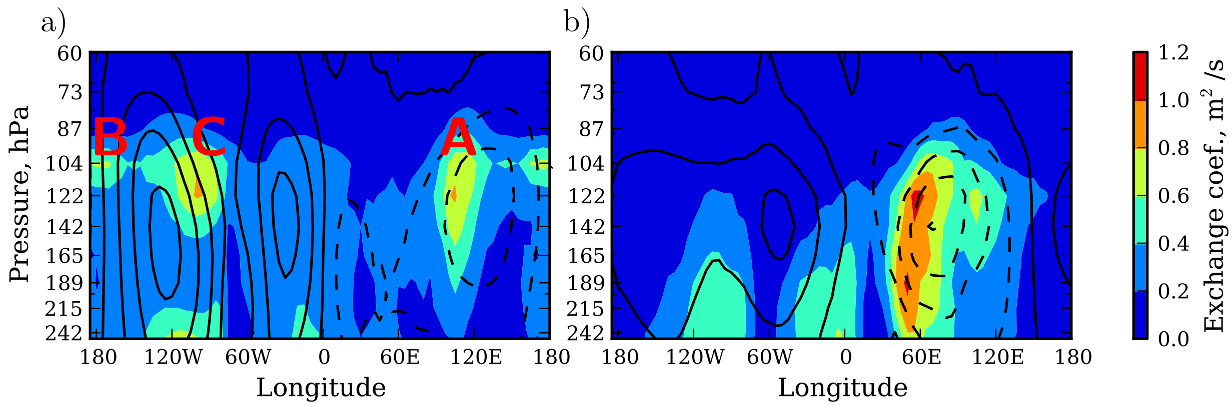

FIG. 3. Climatologically averaged exchange coefficient K_{H} according to the rL scheme for a) DJF and b) JJA averaged over 10°S–10°N using ERA-Interim data from 1989 to 2009. Black contours show zonal wind. The labeled regions ("A", "B", "C") of mixing in panel a) are referred to in the text.

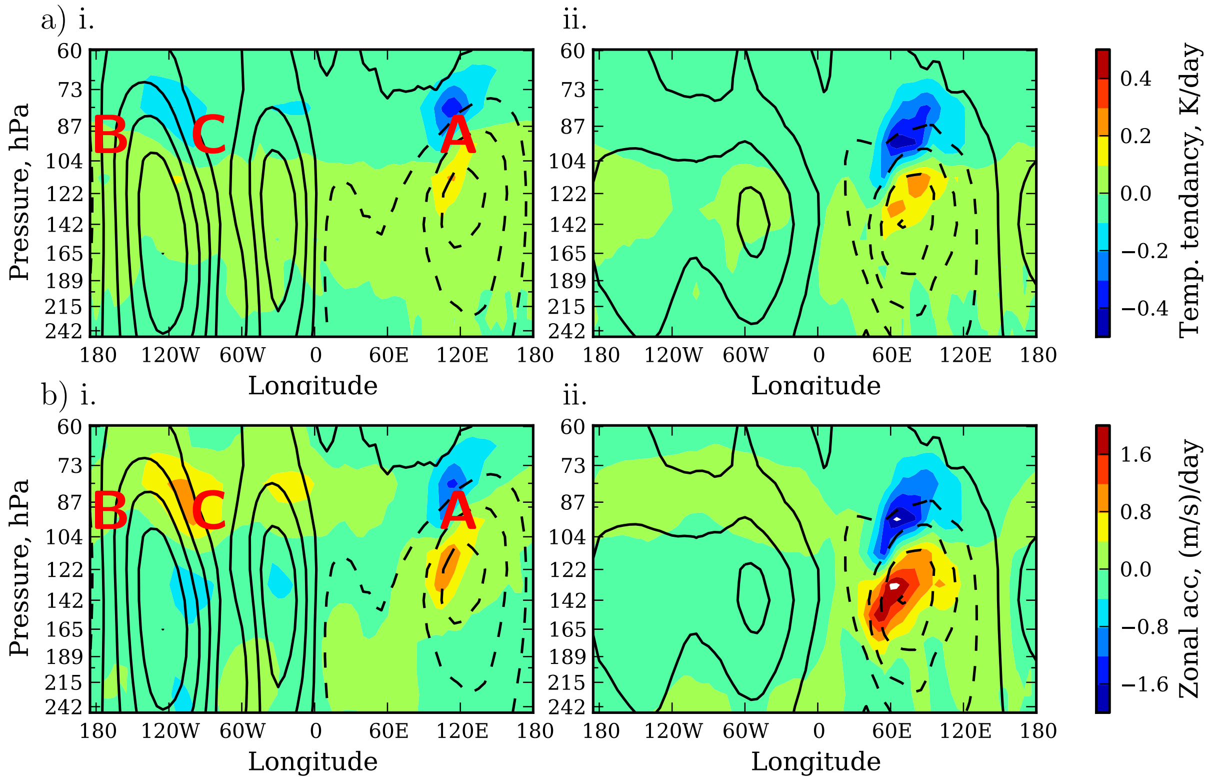

FIG. 4. a) Temperature tendency Q and b) zonal acceleration X due to the forcing terms arising from the revised Louis mixing scheme for i) DJF and ii) JJA averaged over 10°S–10°N using ERA-Interim data from 1989 to 2009. Black contours show zonal wind. The regions A, B and C shown here are the same as those in Figure 3.

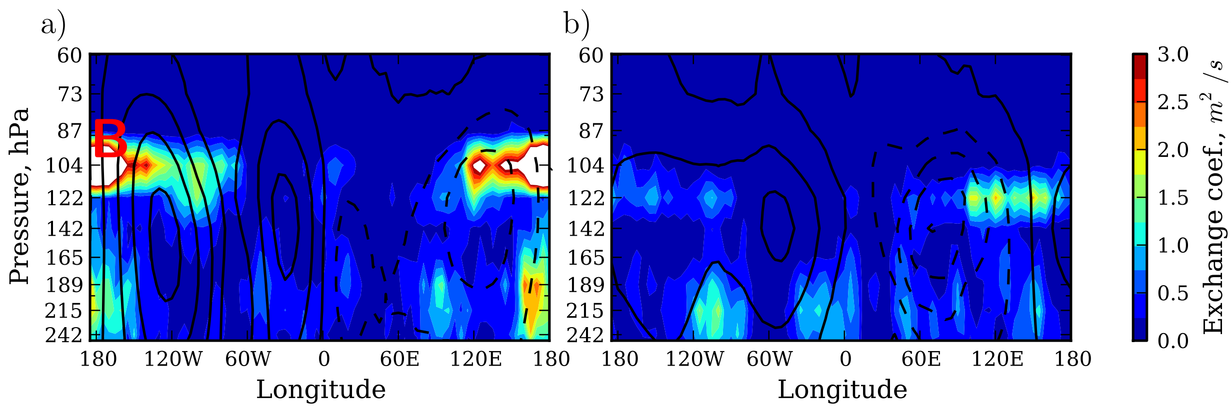

FIG. 5. As in Figure 3 but using the MO scheme. Region B is marked in the same location as in Figure 3a. Note that the color scale has been chosen to saturate before the maximum K_H in the DJF Pacific (approximately 10 $m^2\,s^{-1}$; regions above 3 $m^2\,s^{-1}$ are shown in white) to highlight the structure of K_H elsewhere in the domain.

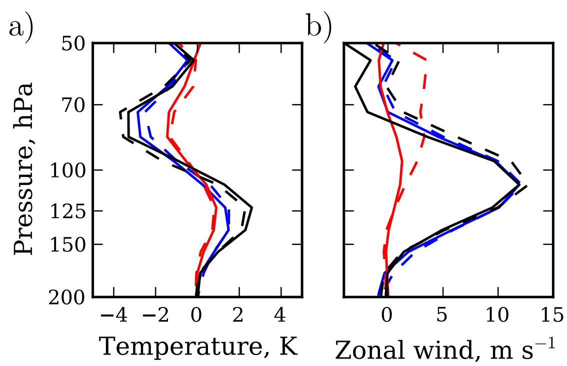

FIG. 6. Zonal average response to zonally symmetric forcings F_X^{sym} (blue solid), F_Q^{sym} (red solid) and both F_X^{sym} and F_Q^{sym} (black solid), in a) temperature and b) zonal wind, averaged over 10°N–10°S, with HS94 background state. Similarly, the responses to the local forcings F_X (blue dashed), F_Q (red dashed) and both F_X and F_Q (black dashed).

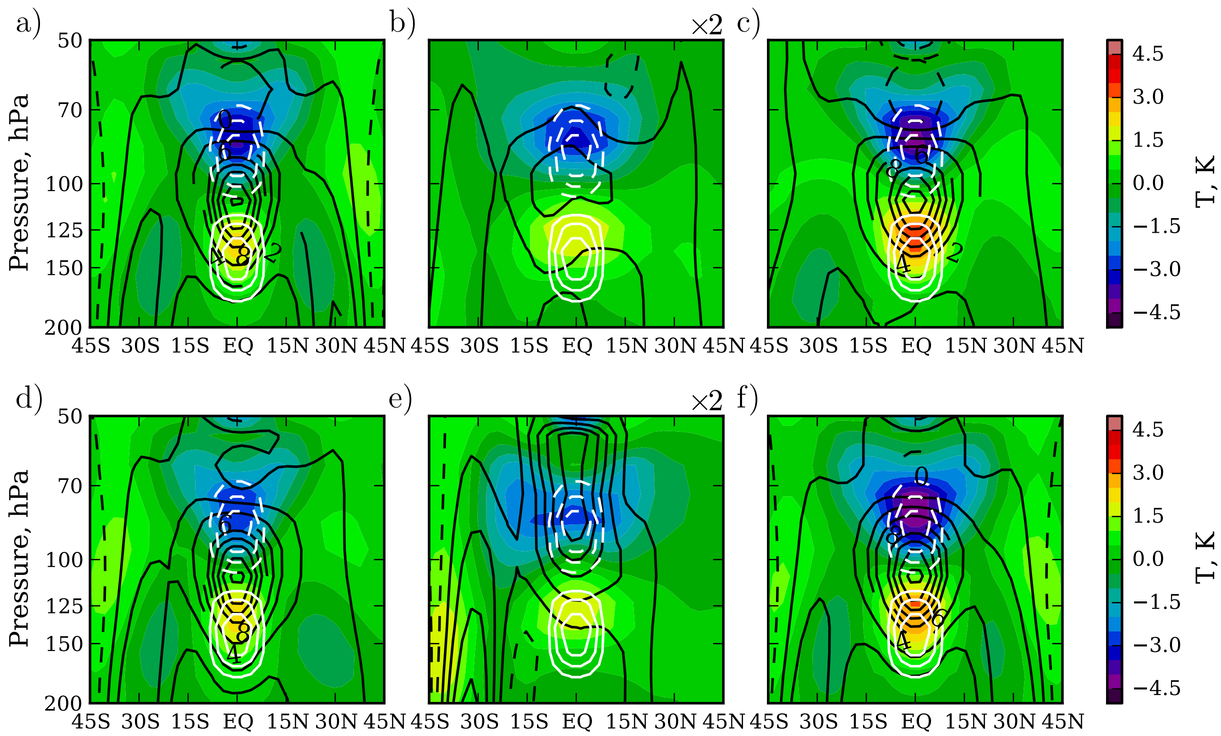

FIG. 7. Zonal mean temperature response $\delta\overline{T}$ (colors) and zonal mean wind response $\delta\overline{u}$ (black contours; contour spacing 2 m s^{-1}, 1 m s^{-1} in b and e) for forcings a) F_X^{sym}, b) F_Q^{sym}, c) both F_X^{sym} and F_Q^{sym}, d) F_X, e) F_Q, and f) both F_X and F_Q, with HS94 background state. The temperature color scale used in b) and e) is half that shown in the color bar. White contours show the structure of the forcing (normalized by amplitude.)

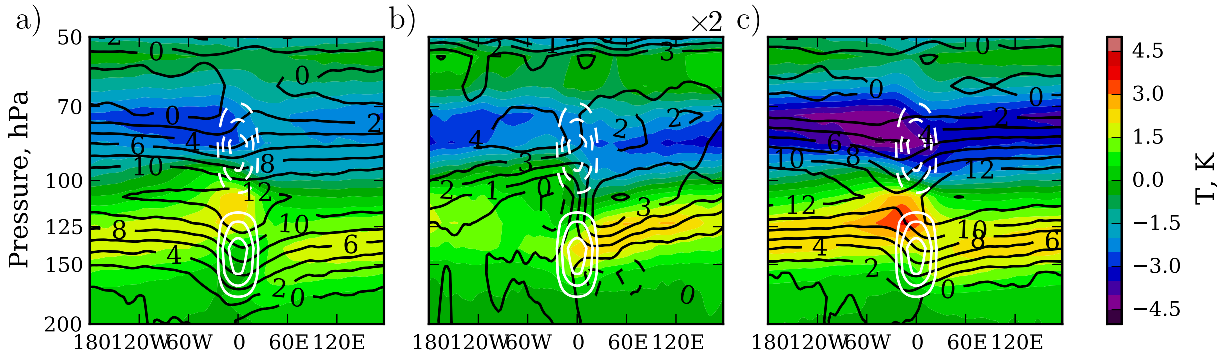

FIG. 8. Inner tropical (10°N–10°S) average temperature response δT (colors) and zonal wind response δu (black contours; contour spacing 2 $\mathrm{m\,s^{-1}}$, 1 $\mathrm{m\,s^{-1}}$ in b) for localized forcings a) F_X, b) F_Q, and c) both F_X and F_Q, with HS94 background state. The temperature color scale used in b) is half that shown in the color bar. White contours show the structure of F_X and F_Q.

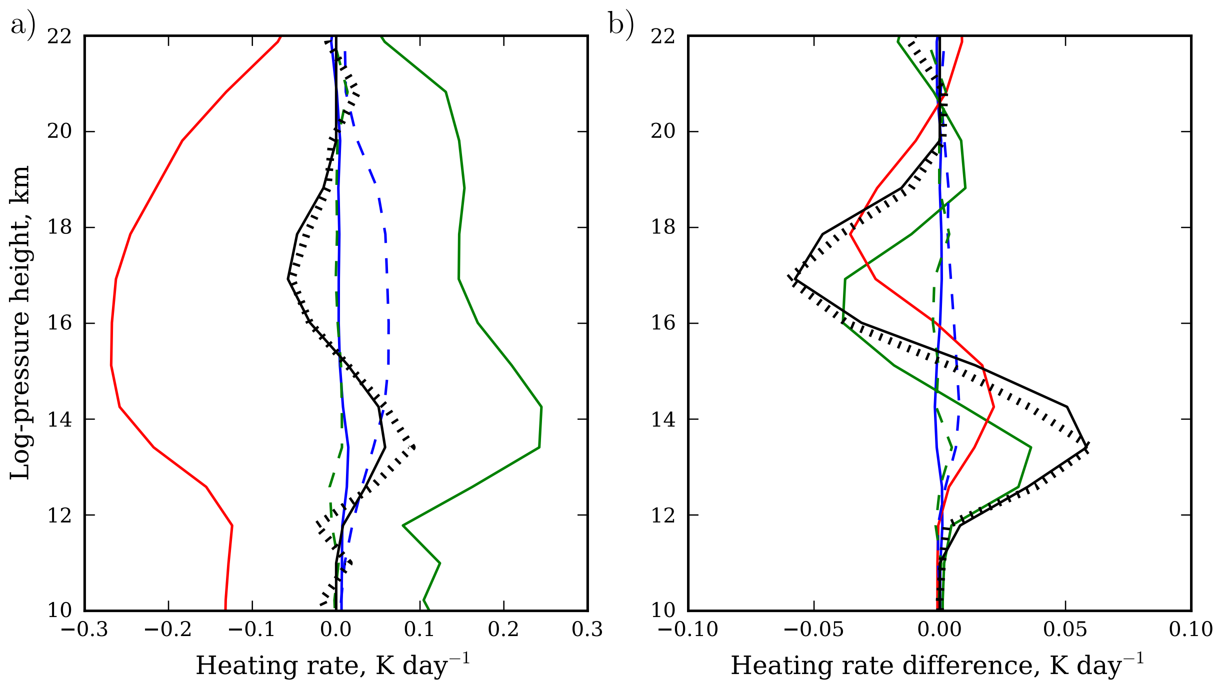

FIG. 9. a) Profiles of the terms in Eq. (5) (the time mean zonal mean buoyancy equation) averaged over $\pm 10°$ for the run forced with F_Q^{sym}; the meridional advection term (blue solid), the vertical advection term (green solid), the meridional eddy heat flux term (blue dashed), the vertical eddy heat flux term (green dashed), the Newtonian cooling term (red) and the imposed heating F_Q^{sym} (black solid) are shown. The sign of all terms except F_Q^{sym} are chosen to put them on the LHS of Eq. (5). The black dotted line shows the sum of all terms that balance the forcing term. b) Profiles of the difference between the forced and unforced runs for each quantity shown in a).

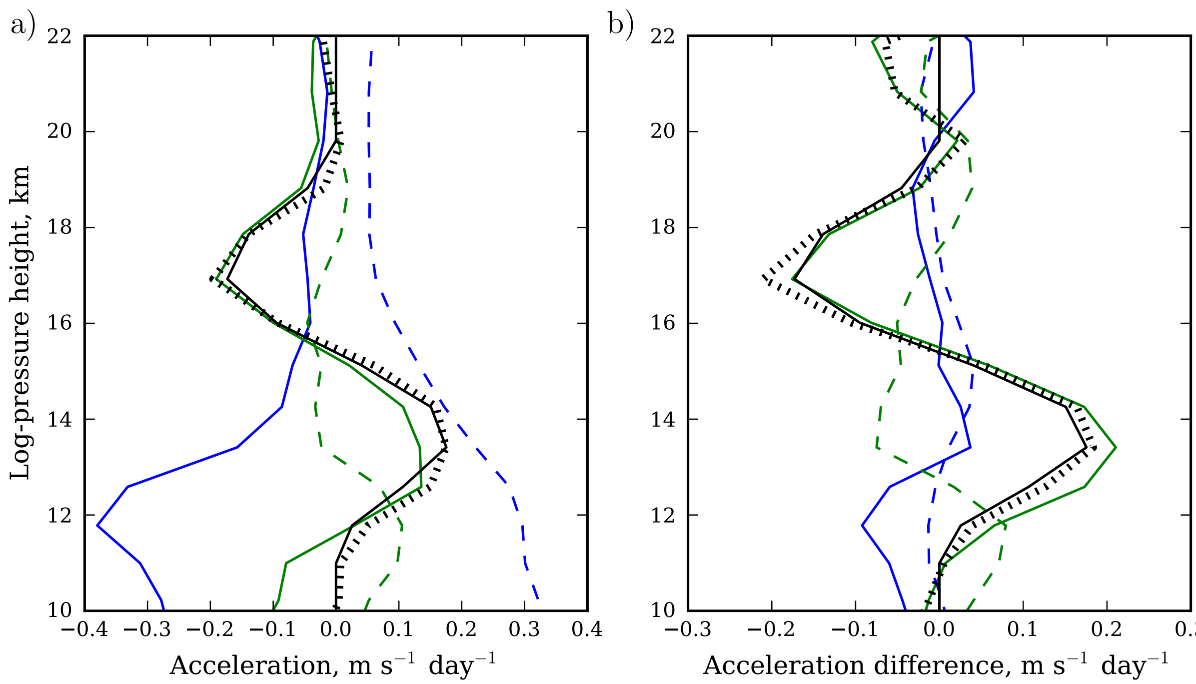

FIG. 10. a) Profiles of the terms in Eq. (9) (the time mean zonal mean zonal momentum equation) averaged over $\pm 10°$ for the run forced with F_X^{sym}; the sum of the meridional advection and Coriolis terms (blue solid), the vertical advection term (green solid), the meridional eddy momentum flux term (blue dashed), the vertical eddy momentum flux term (green dashed) and the imposed zonal acceleration F_X^{sym} (black solid) are shown. The black dotted line shows the sum of all terms that balance the forcing term. The sign of all terms except F_X^{sym} are chosen to put them on the LHS of Eq. (9). b) Profiles of the difference between the forced and unforced runs for each quantity shown in a).

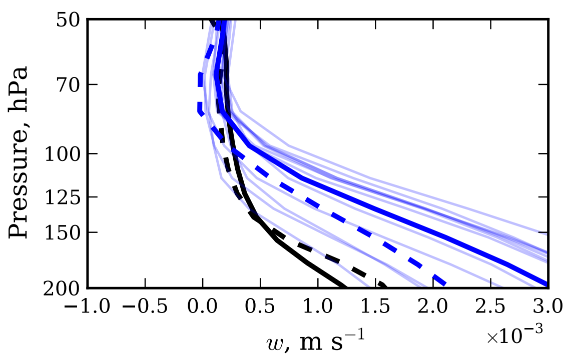

Fig. 11. Mean vertical velocity $\overline{w}$ averaged over 10°N to 10°S (solid lines) and at the equator (dashed lines) for the HS94 run with no imposed forcing (black), and for ERA-Interim averaged over 1979 to 2012 (blue lines, thick line is average, thin lines are climatological annual cycle monthly averages.)

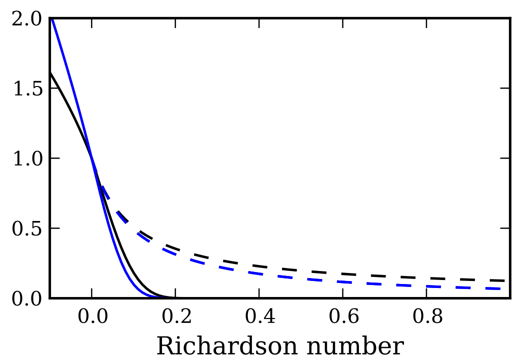

FIG. 12. $f_{\mathrm{M}}(Ri)$ (black) and $f_{\mathrm{H}}(Ri)$ (blue) in the MO scheme (solid) and rL scheme (dashed).

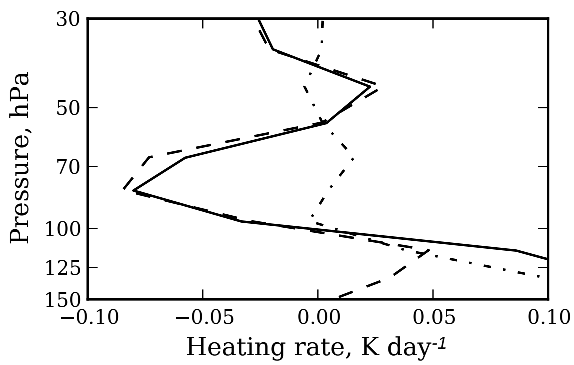

Fig. 13. Zonal mean ERA-Interim residual diabatic temperature tendency (solid), the temperature tendency due to vertical mixing as parametrised by the rL scheme (dashed), and the difference between these curves (dash-dot) averaged over January 2001 over 10°S–10°N.